

scale that depends on the shear rate. The autocorrelation function may also be plotted against a dimensionless time, namely the amount of strain $\dot{\gamma}T$ (Fig. 6C). When plotted this way, one sees that the deformation remains correlated for higher strains at higher Wi . Larger changes in conformation occur at higher Wi , and more strain is apparently required to produce these changes. Empirically, the data for all Wi may be approximately, but not exactly, collapsed by plotting the autocorrelation versus $\dot{\gamma}T/(Wi)^{2/3}$.

We have presented experimental data on the conformational dynamics of individual polymer molecules in steady shear flow. Possible improvements in the technique include better spatial and temporal resolution and specific labeling of portions of the polymer. The ability to clearly distinguish the ends of the chain should allow the tumbling dynamics to be studied in greater detail. In future studies, it is expected that these types of measurements may be extended to time-dependent (transient) flows and to the study of semi-dilute and entangled polymer solutions. Such experiments, in conjunction with the development of accurate molecular models, should reveal many details of the molecular processes that underlie non-Newtonian rheological effects. This approach should be useful for rigorously testing polymer physics models and lay the foundation for a complete microscopic understanding of the rheology of polymer solutions.

References and Notes

1. P. Rouse, *J. Chem. Phys.* **21**, 1272 (1953); B. Zimm, *ibid.* **24**, 269 (1956); A. Peterlin, W. Heller, M. Nakagaki, *ibid.* **28**, 470 (1958); H. Warner, *Ind. Eng. Chem. Fundam.* **11**, 379 (1972); E. Hinch, *J. Fluid Mech.* **75**, 765 (1976); J. Magda, R. Larson, M. Mackay, *J. Chem. Phys.* **89**, 2504 (1988); L. Wedgewood and H. Ottinger, *J. Non-Newtonian Fluid Mech.* **27**, 245 (1988); L. Wedgewood, D. Ostrov, R. Bird, *ibid.* **40**, 119 (1991).
2. W. Kuhn and H. Kuhn, *Helv. Chim. Acta.* **26**, 1394 (1943); D. E. Keyes and F. H. Abernathy, *J. Fluid Mech.* **185**, 503 (1987).
3. T. Liu, *J. Chem. Phys.* **90**, 5826 (1989); P. Doyle, E. Shaqfeh, A. Gast, *J. Fluid Mech.* **334**, 251 (1997); P. Doyle, E. Shaqfeh, *J. Non-Newtonian Fluid Mech.* **76**, 78 (1998).
4. J. Lumley, *Annu. Rev. Fluid Mech.* **1**, 367 (1969).
5. P. G. de Gennes, *J. Chem. Phys.* **60**, 5030 (1974).
6. R. Larson, *Constitutive Equations for Polymer Melts and Solutions* (Buttersworths, New York, 1988).
7. F. Cottrell, E. Merrill, K. Smith, *J. Polym. Sci. Polym. Phys. Ed.* **7**, 1415 (1969); A. Link and J. Springer, *Macromolecules* **26**, 464 (1993).
8. E. C. Lee, M. J. Solomon, S. J. Muller, *Macromolecules* **30**, 7313 (1997).
9. P. Lindner and R. Oberthur, *Colloid Polym. Sci.* **266**, 886 (1988).
10. G. G. Fuller and L. G. Leal, *Rheol. Acta* **19**, 580 (1980); J. Bossart and H. Ottinger, *Macromolecules* **30**, 5527 (1997).
11. D. E. Smith and S. Chu, *Science* **281**, 1335 (1998); T. T. Perkins, D. E. Smith, S. Chu, *ibid.* **276**, 2016 (1997); _____, in *Flexible Chain Dynamics in Elongational Flow*, H. Kausch and T. Nguyen, Eds. (Springer-Verlag, Berlin, in press).
12. A 1.3 cm by 2.5 cm glass slide glued to a piece of Plexiglass (acrylic plastic) was positioned above a 2.5 cm by 5.7 cm by 1.5 cm channel by three micrometer

- screws. The plate was held against the screws by a stiff spring, allowing one to level the plates and to adjust the size of the gap between them (with <5% variation). The bottom plate, which acted as an optical window, was a 1.5 cm by 5.7 cm, no. 2 glass coverslip. The top plate was connected to the channel by a translation stage that was leveled relative to the bottom plate by a fourth micrometer screw. The translation stage was driven by an optically encoded dc motor moving at speeds of 10 to 200 $\mu\text{m/s}$ with $\sim 2\%$ root mean square variation over 2.4 cm of travel.
13. λ -DNA (Gibco BRL, Gaithersburg, MD) was labeled with YOYO-1 (Molecular Probes, Eugene, OR) at a dye/base pair ratio of 1:4 for >1 hour. The persistence length of native DNA is ~ 53 nm [C. Bustamante, J. Marko, E. Siggia, S. Smith, *Science* **265**, 1599 (1994)] and its hydrodynamic diameter is ~ 2 nm [R. Pecora, *ibid.* **251**, 893 (1991)]. When labeled with YOYO, the contour length increases to ~ 22 μm [T. T. Perkins, D. E. Smith, R. G. Larson, S. Chu, *ibid.* **268**, 83 (1995)]. Experiments were performed at $\sim 20^\circ\text{C}$ in a pH 8 buffer consisting of 10 mM tris-HCl, 2 mM EDTA, 10 mM NaCl, 4% β -mercaptoethanol, glucose oxidase (~ 50 $\mu\text{g/ml}$) and catalase (~ 10 $\mu\text{g/ml}$), ~ 10 to 18% (w/w) glucose, and 40 to 55% (w/w) sucrose. In this solution, where the free oxygen has been minimized, the photobleaching of the molecules during the measurements was found to be negligible. The viscosity of each solution was measured and adjusted by varying the sugar concentrations.
14. Molecules were epi-illuminated by a 100 W mercury arc lamp (Zeiss) with a 470 ± 32 nm bandpass excitation filter and a 500-nm long-pass dichroic mirror and imaged with a $\times 60$, 1.2 numerical aperture water immersion objective (Nikon), a 160-mm-to-infinity-corrected conversion lens (Zeiss), a 40-cm tube lens, a 515-nm long-pass emission filter, a microchannel plate intensifier (Hamamatsu), and a video camera (Phillips CCD).
15. The concentration was kept very low so that the dynamics of isolated, noninteracting molecules could be observed. Typically it was 10^4 to 10^5 times lower than the concentration (c^*) at which coiled molecules begin to overlap.

16. We determined that $\tau = 6.3$ s in the 60-cP solution and 19 s in the 220-cP solution by analyzing the relaxation of >40 molecules that were extended by $>30\%$ when the flow was stopped. τ was determined by fitting to the function $x(t)^2 = c \exp(-t/\tau) + 2R_G$, where τ , c , and R_G were free parameters.
17. E. Atkins and M. Taylor, *Biopolymers* **32**, 911 (1992).
18. Also, the birefringence does not directly correspond to the extension but rather the ordering of portions of the chain along the polarization axis.
19. D. E. Smith, T. T. Perkins, S. Chu, *Macromolecules* **29**, 1372 (1996).
20. The FFT was calculated after subtracting the mean extension from all of the data points and multiplying the data by a Welch window function [W. H. Press et al., *Numerical Recipes in C* (Cambridge Univ. Press, Cambridge, 1988), p. 442]. The PSD for all of the data sets at the same $\dot{\gamma}$ and η were averaged together and normalized according to Parseval's theorem.
21. G. Jeffery, *Proc. R. Soc. Lond. Ser. A* **102**, 161 (1922).
22. The maximum frequency that can be resolved is determined by the sampling rate, typically 0.1 s. The minimum frequency is determined by the length of the run, typically 150 s for $\dot{\gamma} > 2$ and as long as 800 s for $\dot{\gamma} = 0.2$.
23. The ratio of the values determined experimentally (16) were close to, but not exactly equal to, the ratio of the solvent viscosities. The deviation from a strict linear proportionality may be due to slight differences in the solvent arising from the differing fractions of water in the two solutions.
24. M. Wang and G. Uhlenbeck, *Rev. Mod. Phys.* **17**, 323 (1945).
25. E. Shaqfeh and J. Hur, personal communication.
26. We acknowledge assistance from T. Perkins with an earlier version of this experiment and helpful comments from J. Hur, R. Larson, T. Perkins, E. Shaqfeh, and B. Zimm. This work was supported in part by the AFOSR and the NSF. D.E.S received support from a fellowship from the NSF Program in Mathematics and Molecular Biology. H.P.B. was supported in part by an NIH biophysics training grant.

3 December 1998; accepted 11 February 1999

How Strong Is a Covalent Bond?

Michel Grandbois,¹ Martin Beyer,² Matthias Rief,^{1,3} Hauke Clausen-Schaumann,¹ Hermann E. Gaub^{1*}

The rupture force of single covalent bonds under an external load was measured with an atomic force microscope (AFM). Single polysaccharide molecules were covalently anchored between a surface and an AFM tip and then stretched until they became detached. By using different surface chemistries for the attachment, it was found that the silicon-carbon bond ruptured at 2.0 ± 0.3 nanonewtons, whereas the sulfur-gold anchor ruptured at 1.4 ± 0.3 nanonewtons at force-loading rates of 10 nanonewtons per second. Bond rupture probability calculations that were based on density functional theory corroborate the measured values.

The mechanical stability of covalent bonds has been investigated indirectly in ensemble measurements or by flow-induced chain frac-

ture in liquids (1). The development of nanoscale manipulation techniques (2) has made it possible to directly address single atoms or molecules and probe their mechanical properties. It has been shown that individual polymers may be stretched between the tip of an AFM cantilever and a substrate surface (3–12). In these studies, polymers were coupled either by specific receptor ligand systems, which were covalently attached to the polymers (8), or by nonspecific adsorption to the tip and the substrate (3,

¹Lehrstuhl für Angewandte Physik, Ludwig-Maximilians-Universität, Amalienstrasse 54, D-80799 München, Germany. ²Institut für Physikalische und Theoretische Chemie, Technische Universität München, Lichtenbergstrasse 4, 85748 Garching, Germany. ³Department of Biochemistry B400, School of Medicine, Stanford University, Stanford, CA 94305–5307, USA.

*To whom correspondence should be addressed.

REPORTS

10–12). Force-extension curves that were recorded during stretching and relaxation revealed a wealth of fingerprintlike features, such as conformational transitions or supermolecular rearrangements (3, 6, 8–12). In our study, we used these well-known fingerprints to identify individual molecules that were covalently attached to both the tip and the substrate. We stretched the molecules until one of the covalent bonds in series ruptured (Fig. 1). By analyzing the bond rupture, we were able to identify the bond that failed.

Upon stretching, polysaccharides such as dextran or amylose undergo a pronounced transition during which the sugar rings switch into a more extended arrangement (3, 8, 12). With amylose, this results in a characteristic plateau at 275 pN with an extension of 0.5 Å per ring unit [Fig. 2A and (12)]. The transition is fully reversible on the time scale of the experiment and thus does not depend on the rate at which the force is increased. Thus, this transition can be used as a molecular strain gauge that can be built into an experiment to report the force that is acting on any point of the molecular bridge. We used this transition to identify those experiments in which only a single polymer is attached between the tip and the substrate. If two or more polymers are stretched simultaneously, the plateau forces add up and either shift the plateau to higher forces or smear it out. Both cases can easily be distinguished from the plateau of a single polysaccharide (13).

In the first set of our experiments, carbodiimide chemistry (14) was used to introduce a symmetric covalent attachment of amylose between the substrate and the tip (Fig. 1B). Both silicon oxide surfaces had been functionalized with amino groups beforehand (15). The activated amylose was first coupled to the substrate surface. Then, the tip was slowly brought into contact with the surface, allowing the polymer to bind to the tip (16). In ~30% of the cases, an individual polymer

was attached. In the other cases, either multiple bonds or no bonds occurred. The tip and the substrate were gradually separated while the force was recorded (Fig. 2). The plateau was analyzed by repeatedly stretching and relaxing the polymer through the conformation transition. After confirming that a single molecule was bound, the force was gradually increased until the molecular bridge ruptured.

The rupture of these single-molecule bridges occurred in multiple irreversible steps (Fig. 2B). As shown in the enlarged section of the curve in Fig. 2B, several peaks at variable but discrete spacing (Fig. 3A) precede the final rupture event, after which the force drops to zero. Because only a single polymer is stretched and the molecular bridge between the tip and the substrate remains intact after the individual rupture events, these multiple bond ruptures reflect the stepwise detachment of the polysaccharide from the surfaces. Given the manner in which a polymer interacts with a surface, it is to be expected that the polysaccharide is bound to the surface in loops and trains (17). With increasing force, the bonds of the loops to the surface thus break one by one, whereas the polymer backbone stays intact (see Fig. 1A). After each detachment, the force drops abruptly because the previously unstretched section can take up the slack and thus increase the length of the stretched polymer bridge (18). A quantitative analysis of the bond rupture force is given in Fig. 3B. At the given force-loading rates of 10 nN/s, the histogram peaks at a value of 2.0 ± 0.3 nN (19).

This finding that it is the attachment that ruptures and not the polymer backbone indicates that the measured bond rupture must be attributed to either of the bonds that are part of the attachment and not part of the polysaccharide. In Fig. 1B, the schematics of the chemistry of the attachment are depicted. Four bonds are unique to the attachment: Si–O, Si–C, C–C, and C–N

bonds. The C–O bond is found in the attachment and in the amylose backbone. At first, it was difficult to decide which of these four different bonds was breaking in our experiment. We ruled out the rupture of the Si–O bond because three of these bonds hold in parallel at the surface. As a first approximation, we correlated the strength of a covalent bond with the ratio of the dissociation energy and the bond length. Considering the enthalpy for dissociation and the bond length (20), we decided that the Si–C bond was the most likely candidate for rupture in our experiment.

This hypothesis was confirmed by a theoretical investigation of the rupture forces for the different kinds of covalent bonds in the system. One-dimensional potential functions for the covalent bonds of interest were derived from high-level density functional calculations of small model mole-

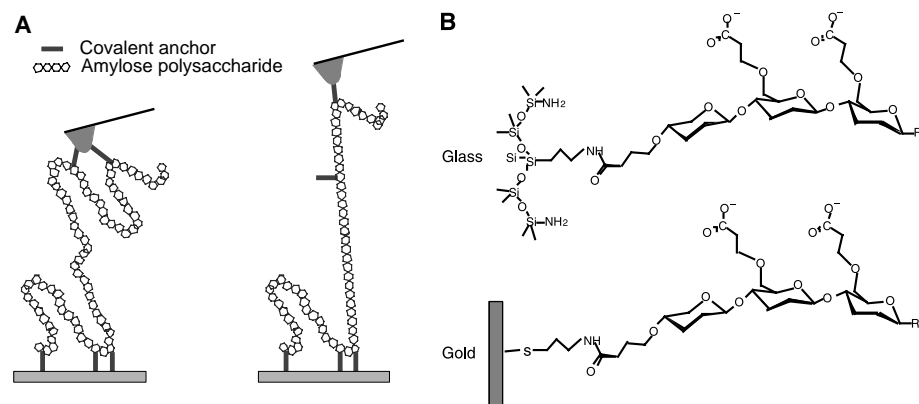


Fig. 1. (A) Stretching of a single polysaccharide chain that is covalently attached to the AFM tip and the substrate. (B) Schematics of the covalent attachment of the amylose by carbodiimide chemistry to glass or Au surfaces, which were both functionalized with amino groups.

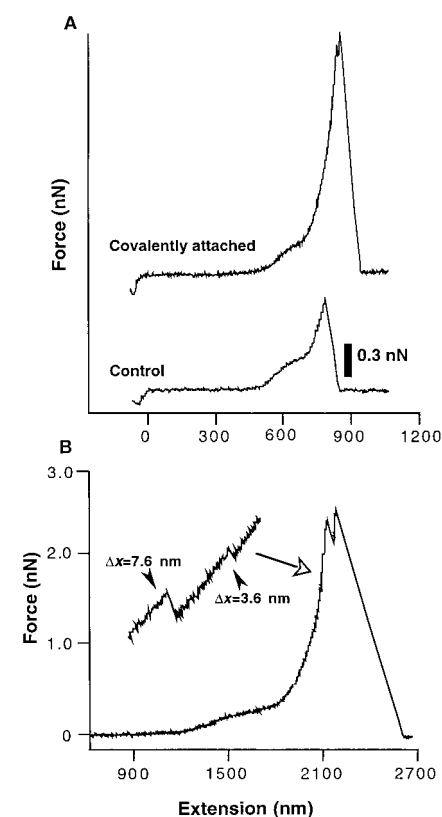


Fig. 2. (A) Force versus extension curve of amylose covalently bound between an AFM tip and a silicon oxide surface. The indentation force was kept below 0.3 nN for each approach. The control force versus extension was measured without treatment of the amylose with EDC or NHS. (B) Measured force versus extension curve of amylose showing multiple ruptures in the high-force regime. The enlarged curve section of the high-force regime shows multiple small-step ruptures leading to elongations (Δx) of the amylose polymer. All the ruptures observed in the force versus extension curves were plotted in the histogram shown in Fig. 3B.

cules, from which one-dimensional Morse potentials were extracted. Adapting the method outlined in (21), temperature- and force-ramp-dependent bond rupture probability densities were calculated (Fig. 4). Theory corroborates our estimate that Si-C is the weakest of all the bonds in question. The absolute values for the calculated bond rupture forces are slightly higher than the experimental values. This difference may reflect solvent effects that were not considered in our calculations. These theoretical values, as well as the experimental results, compare well to the value obtained by a resistance test on a small polymer specimen [3 nN (1)] or by a flow-induced fracture of single polymer chains [2.5 to 13.4 nN (1)].

We compared the bond strength of the Si-C bond to the strength of the attachment of the polymer through S to Au (Fig. 3C). The experimental setup and the protocol were identical to the previous experiments, except that the substrate was an evaporated Au surface, which was activated with an aminothioli. The attachment to the tip was unaltered. As seen in Fig. 3D, this replacement resulted in a reduction of the bond rupture force to values of 1.4 ± 0.3 nN. In control experiments, where the polysaccharide was chemically coupled to the Au substrate but not to the tip, the same nonspecific attachment forces of 0.8 ± 0.2 nN were measured as in the silicon oxide control experiments (Fig. 3, C and E). Because the nonspecific interaction between the tip and the polysaccharide was probed in both cases, this agreement was to be expected. This value is also consistent with previously measured values on comparable surfaces (8).

In the symmetric silicon oxide experiment, the measured rupture force could be clearly attributed to the Si-C bond, whereas the S-Au rupture experiments leave room for speculation. Whether this measured value of 1.4 nN represents the rupture of the Au-S bond or the extraction of the S-bonded Au atoms from the metal surface remains unclear.

Although chemical compounds play a dominant role in material sciences, the

forces that chemical bonds can withstand could previously not be directly measured in experiments. The experiments reported here demonstrated that the individual chemical bonds can be probed in mechanical experiments. An important feature of such experiments is the mechanical activation of chemical bonds (here in the simplest form as bond rupture), which can now be studied on an individual basis.

Fig. 4. Bond rupture probability densities were derived in three steps of theoretical modeling. First, high-level density functional calculations (25) of small model molecules in the gas phase were used to derive potential functions that accounted for the deformations and hybridizations caused by the application of force. Pulling on the terminating H atoms (for example, $H_3SiCH_2CH_3$) was simulated by a so-called "relaxed potential energy surface scan." Starting from a fully optimized geometry, a series of constrained geometry optimizations was performed in which the distance $r(H-H)$ was elongated in steps of 0.1 Å. The energy of the otherwise relaxed molecule was calculated, which yielded a potential for the deformation of the model molecule. The force that corresponds to a certain elongation is the gradient of the potential. For kinetic modeling, the quantum mechanically calculated potential was fitted by a Morse potential (20) $V = D_e[1 - \exp[-b(r - r_e)]]^2$, where D_e is the bond dissociation energy, b is chosen so that V has the same maximum slope as the calculated potential, and r_e is the equilibrium distance. In the kinetic model, the rupture rate constant $\eta(F)$ was calculated as a function of the applied force. Under force, V is deformed to the effective potential $V_{eff} = V - F(r - r_e)$ (inset), which in turn yields the parameters for the Arrhenius rate constant law $\eta(F) = A \exp(-E_A/kT)$, where A is the Arrhenius A factor, E_A is the activation energy, k is the Boltzmann constant, and T is temperature (21). This rate function $\eta(F)$ was numerically convoluted with a typical experimental load of 10 nN/s, resulting in the bond rupture probability density as a function of force. Results are shown for the model molecules of $H_3SiCH_2CH_3$, H_3SiOCH_3 , $H_3CCH_2CH_3$, H_3COCH_3 , and H_3CNHCH_3 . The Si-C bond in $H_3SiCH_2CH_3$ comes closest to the experimental values of rupture force.

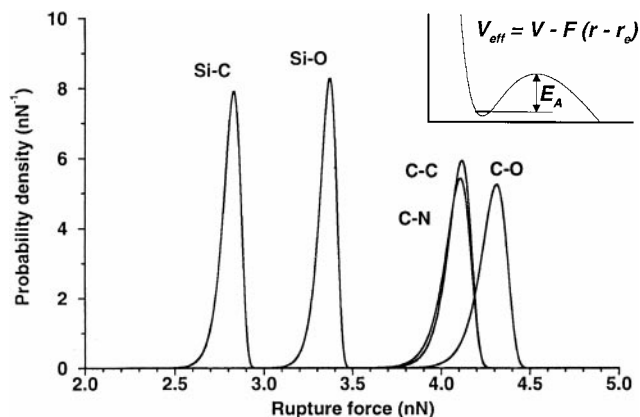
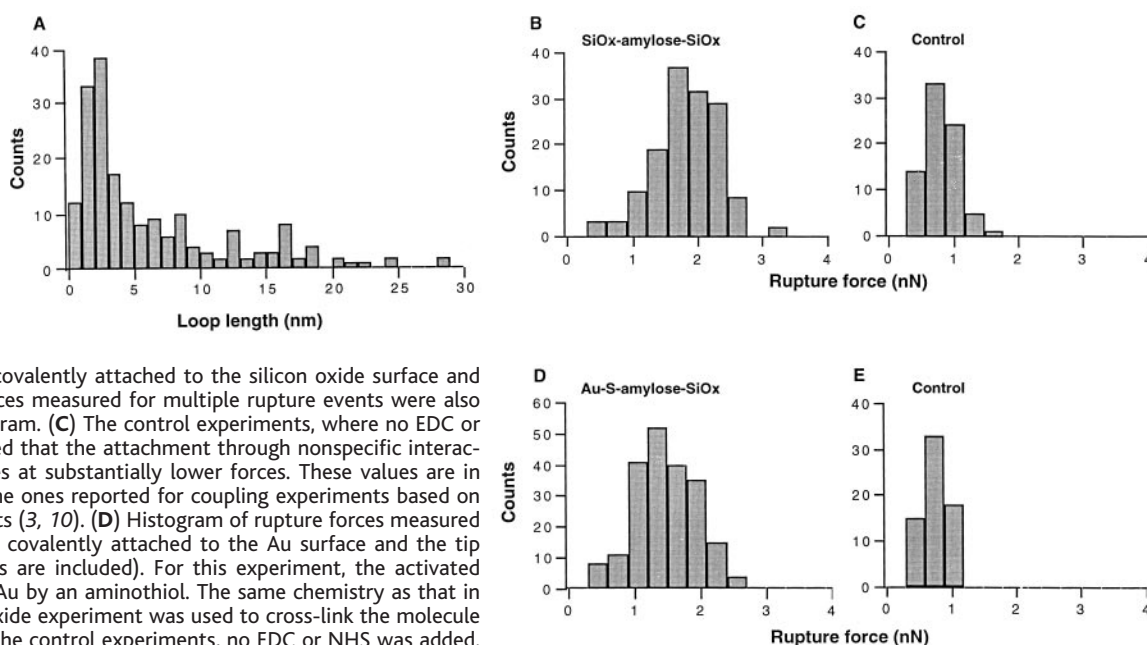


Fig. 3. (A) Histogram of the length gain after the events were measured in the force versus extension curves showing multiple ruptures for amylose, which was covalently attached to the silicon oxide surface and the tip. Polymer elongations were measured with an error of ± 2 Å. (B) Histogram of rupture forces measured for amylose covalently attached to the silicon oxide surface and the tip. The rupture forces measured for multiple rupture events were also considered in the histogram. (C) The control experiments, where no EDC or NHS was added, revealed that the attachment through nonspecific interaction of polymer ruptures at substantially lower forces. These values are in good agreement with the ones reported for coupling experiments based on noncovalent attachments (3, 10). (D) Histogram of rupture forces measured for amylose, which was covalently attached to the Au surface and the tip (multiple rupture events are included). For this experiment, the activated amylose was bound to Au by an aminothioli. The same chemistry as that in the symmetric silicon oxide experiment was used to cross-link the molecule to the AFM tip. (E) For the control experiments, no EDC or NHS was added. The nonspecific adhesion forces are comparable to those in Fig. 3C.



References and Notes

1. P. I. Vincent, *Polymer* **13**, 557 (1972); J. A. Odell et al., *J. Polym. Sci.* **24**, 1889 (1986).
2. G. Binnig, C. F. Quate, Ch. Gerber, *Phys. Rev. Lett.* **56**, 930 (1986); S. P. Jarvis, H. Yamada, S.-I. Yamamoto, H. Tokumoto, J. B. Pethica, *Nature* **384**, 247 (1996); M. Radmacher, M. Fritz, H. G. Hansma, P. K. Hansma, *Science* **265**, 1577 (1994).
3. H. Lee et al., *Adv. Mater.* **3**, 316 (1998).
4. U. Dammer et al., *Biophys. J.* **70**, 2437 (1995).
5. P. Hinterdorfer, W. Baumgartner, H. J. Gruber, K. Schilcher, H. Schindler, *Proc. Natl. Acad. Sci. U.S.A.* **93**, 3477 (1996).
6. S. B. Smith, Y. Cui, C. Bustamante, *Science* **271**, 795 (1996).
7. P. Cluzel et al., *ibid.*, p. 792.
8. M. Rief, F. Oesterhelt, B. Heymann, H. E. Gaub, *ibid.* **275**, (1997).
9. M. Rief, M. Gautel, F. Oesterhelt, J. M. Fernandez, H. E. Gaub, *ibid.* **276**, 1109 (1997).
10. A. F. Oberhauser et al., *Nature* **393**, 181 (1998).
11. X. Châtelier, T. J. Senden, J.-F. Joanny, J.-M. Di Meglio, *Europhys. Lett.* **41**, 303 (1998).
12. P. E. Marszalek, A. F. Oberhauser, Y.-P. Pang, J. M. Fernandez, *Nature* **396**, 661 (1998).
13. All of the evaluated molecules show a transition at 275 pN, and the deformation traces scale linearly with the contour length. As has been previously shown (3, 8, 12), this is a strict criterion that applies to the stretching of a single polysaccharide.
14. S. Löfas and B. Johansson, *J. Chem. Soc. Chem. Commun.* **566**, 1526 (1990).
15. Microscope slides (Menzel Gläser, Braunschweig, Germany) and AFM tips (Park Scientific Instruments, Sunnyvale, CA) were incubated with *N*'-[3-(trimethoxysilyl)-propyl]-diethylenetriamine (Aldrich) at 90°C for 15 min, rinsed in ethanol, and rinsed in water. The tips and the surfaces were then cured for 30 min at 120°C. The Au surfaces, which were functionalized with amino groups, were prepared by incubating a freshly evaporated Au surface for 30 min with a 100 mM aqueous solution of mercaptoethylamine (Sigma). Carboxymethylated amylose (1 mg/ml) was allowed to react with 1-ethyl-3-(3-dimethylaminopropyl) carbodiimide (EDC) (20 mg/ml) and *N*-hydroxysuccinimide (NHS) (10 mg/ml) (all from Sigma) in phosphate-buffered saline (PBS) at pH 7.4 to introduce succinimide reactive groups along the polysaccharide chain (14). This activated polymer was then incubated for 5 min with the amino-silanized glass surface and thoroughly rinsed to remove noncovalently bound molecules. The AFM tip was approached and allowed to react with the amylose so that force versus elongation measurements of the polysaccharide could be recorded. All measurements were recorded in PBS at pH 7.4.
16. To minimize the attachment of multiple amylose strands, which typically occurred at the first approaches of the tip, we let the tip approach the surface step by step, retracting the tip partly after each approach until a binding event was observed upon pulling back. In this so-called "fly fishing mode" (8), undesirable multiple bonds can be efficiently avoided.
17. P. G. De Gennes, *J. Phys.* **37**, 1445 (1976).
18. The histogram of the length increase of the amylose strand upon each of these multiple ruptures ranges from 6 to 600 Å. The lower limit of these values is comparable to the length of a stretched sugar ring. Hence, the attachment of a single glucose ring to the surface is capable of holding the entire load applied to the polymer. These steps would result in a plateau if the detachment would be an equilibrium reaction, for example, if the chemical bond could reform before the polymer is pulled away far enough from the surface. Because the detachment of the polymer from the surface is irreversible on the time scale of the experiment and because the AFM has this high spatial resolution, we still see all steps individually (even the small ones, as shown in the enlarged section of the curve in Fig. 2B). The larger steps in the histogram may reflect the unbinding of loops.
19. There are several possible contributions to the width of the distribution. One source is the intrinsic prob-

- ability distribution for bond rupture. Different angles at which the bonds are loaded may contribute to the broadening of the recorded histogram as well. The rupture force is expected to depend on the loading rate as recently demonstrated for the biotin-streptavidin pair (22). This effect was not considered here.
20. Enthalpy of dissociation (in kilojoules per mole) and bond length (in picometers), respectively, are given for the following covalent bonds: Si-C, 318 and 185; Si-O, 452 and 166; C-C, 346 and 154; C-O, 356 and 143; and C-N, 305 and 147 [J. E. Huheey, *Anorganische Chemie* (Walter de Gruyter, Berlin, ed. 3)].
21. E. Evans and K. Ritchie, *Biophys. J.* **72**, 1541 (1997).

22. R. Merkel, P. Nassoy, A. Leung, K. Ritchie, E. Evans, *Nature* **397**, 21 (1999).
23. A. D. Becke, *J. Chem. Phys.* **1993**, 5648 (1993).
24. Gaussian 94, Revision D.4, M. J. Frisch et al. [Gaussian, Pittsburgh, PA (1995)].
25. Computations were done with the B3LYP (23) density functional method in conjunction with the D95(d) basis set as implemented in the Gaussian 94 (24) program package on a DEC Alpha 500 workstation.
26. This work was supported by the Deutsche Forschungsgemeinschaft and the Natural Sciences and Engineering Research Council of Canada.

23 December 1998; accepted 5 February 1999

Adaptation of Bulk Constitutive Equations to Insoluble Monolayer Collapse at the Air-Water Interface

J. Patrick Kampf,¹ Curtis W. Frank,^{1*} Eva E. Malmström,² Craig J. Hawker^{2*}

A constitutive equation based on stress-strain models of bulk solids was adapted to relate the surface pressure, compression rate, and temperature of an insoluble monolayer of monodendrons during collapse at the air-water interface. A power law relation between compression rate and surface pressure and an Arrhenius temperature dependence of the steady-state creep rate were observed in data from compression rate and creep experiments in the collapse region. These relations were combined into a single constitutive equation to calculate the temperature dependence of the collapse pressure with a maximum error of 5 percent for temperatures ranging from 10° to 25°C.

Changing the dimensionality of a system can alter its physical properties. For example, many thin polymer films have a glass transition temperature that is much lower than that of the bulk material (1), and two-dimensional (2D) melting may occur through a fundamentally different mechanism than the melting of bulk solids (2). Despite the inherent differences between 2D and 3D systems, concepts developed for bulk materials can often be extended to describe 2D assemblies. Specifically, the study of monolayer rheology has demonstrated the applicability of continuum concepts to pseudo-2D systems (3–5). In addition, investigators have studied the response of Langmuir films to various forms of deformation and have observed elastic (6), viscous (7), and viscoelastic (8) behavior that is analogous to the deformation response of bulk materials. We explored the applicability of phenomenological models developed from the mechanical behavior of bulk solids to the dynamic response of pseudo-2D monolayers at the air-water interface.

Surface pressure π versus area A isotherms of Langmuir films are most often thought of as 2D analogs to pressure-volume isotherms of bulk materials, and an equilibrium thermodynamic relation between π and A is assumed. Generally speaking, however, π - A isotherms reflect dynamic, rate-dependent measurements. The parts of the π - A isotherm that will be most affected by the compression rate are those that describe monolayer behavior with long relaxation times. For example, monolayer collapse often occurs in the regime where compression rate becomes an important factor. Several authors have examined the effect of compression rate and temperature T on the collapse of insoluble monolayers. Kato and coworkers (9) have shown that compression rate and T alter the collapse pressure of fatty acid monolayers, but they focus mainly on the importance of maintaining a constant strain rate rather than developing a constitutive equation. Duran and coworkers (10) have also examined the effect of compression rate and T within the monolayer collapse region of liquid-crystalline polymers, but most of their quantitative work concentrates on relating these parameters to the stress relaxation times. By splitting π into equilibrium and dynamic components,

¹Department of Chemical Engineering, Stanford University, Stanford, CA 94305-5025, USA. ²IBM Almaden Research Center, San Jose, CA 95120-6099, USA.

*To whom correspondence should be addressed.